



Removal of free cyanide from aqueous solutions by pine cone scale (PCS)

Ali Behnamfard^{a,*}, Rasool Alaei^a, Kamran Chegini^a, Francesco Veglio^b

^aFaculty of Engineering, University of Birjand, South Khorasan, Iran, Tel. +989151603400, email: behnamfard@birjand.ac.ir (A. Behnamfard), Tel. +989156625940, email: alaeirasool@birjand.ac.ir (R. Alaei), Tel. +989389783122, email: kamranchechini@birjand.ac.ir (K. Chegini)

^bDepartment of Industrial and Information Engineering and Economics, University of L'Aquila, 67040 Monteluco di Roio, L'Aquila, Italy, Tel. +39 0862 434236, Fax +39 0862 434203, email: francesco.veglia@univaq.it (F. Veglio)

Received 9 July 2018; Accepted 2 January 2019

ABSTRACT

The removal of free cyanide from aqueous solutions was studied by adsorption onto PCS. The chemical composition of PCS was determined to be 48.91% C, 6.12% H, 0.5% N and 44.47% O. The BET surface area, total pore volume and average pore diameter of the sample were determined to be 0.657 m²/g, 0.020114 cm³ g⁻¹ and 122.41 nm, respectively. The N₂ adsorption isotherm resembled to the Type III standard adsorption isotherms proposed by IUPAC. The SEM-WDX analysis indicates that PCS is a carbon based adsorbent and FTIR analysis confirmed the presence of acidic and basic surface functional groups on its surface. The equilibrium studies showed that the loading capacity of PCS towards CN⁻ increases from 1.16 to 6.64 mg/g and the removal percentage decreases from 87.5% to 25% by increasing initial CN⁻ concentration from 26 to 531 mg/L. The equilibrium and kinetic data were best modeled by Redlich-Peterson isotherm and Pseudo-second order kinetic models, respectively. The basic surface functional groups play the main role in the adsorption of CN⁻ onto the PCS and the rate limiting step was determined to be film diffusion. The study revealed that PCS can be an effective and economically feasible biosorbent for the removal of CN⁻.

Keywords: Cyanide; Adsorption, Pine cone scale; Isotherm; Kinetics

1. Introduction

Wastewaters from various industries such as gold ore processing, coke making, metal cleaning, plating, electroplating, steel tempering, pharmaceuticals, photography, plastics, oil refining etc. generally contain different concentrations of free CN and metal-CN complexes [1]. Releasing of CN contaminated wastewaters into the environment can negatively affect living organisms [2]. CN can enter easily into the body in various ways, by the mucous membrane of the respiratory tract, through the skin especially the wet one and gastrointestinal tract. CN is a rapidly acting poison since it disrupts the process of cellular respiration. The brain and the heart muscle are the most sensitive tissues to

CN toxicity since they have the fastest metabolism of oxygen. The lethal dose of CN for an adult human is 1.5 mg/kg of body weight [3]. Nonetheless, prolonged exposure to CN can lead to various diseases such as hypothyroidism, kidney damage and miscarriages. Hence, CN contaminated wastewaters must be treated before releasing to the environment. This can be performed by different methods such as electrowinning, hydrolysis-distillation, AVR, oxidation, solvent extraction, ion exchange and adsorption [4]. Adsorption is one of the most versatile and widely used methods for wastewater treatment due to efficiency, cost effectiveness and eco-friendliness. Activated carbon as the most versatile adsorbent is a good option for CN⁻ removal from wastewaters, but its application is restricted due to high operating costs of the process [4–6]. Hence, research interests have centered on finding natural, low-cost, readily

*Corresponding author.

available and effective adsorbent for CN^- removal [7–9]. In this context, agricultural wastes can be good option for CN^- removal.

Annually a huge amount of pine cones are produced as agricultural by-product all over the world. The pine cone is an organ on plants in the division conifers [10,11]. The name “cone” derives from its geometric cone shape. Each cone is composed of a large number of woody scales. The PCS is composed of epidermal and sclerenchyma cells which contain cellulose, hemicelluloses, lignin, rosin and tannins in their cell walls. PCS has been used as a low-cost and a readily available adsorbent for removal of various organic pollutants. The adsorption of textile anionic dyes (Acid Black 26, Acid Green 25 and Acid Blue 7) from colored wastewater has been investigated onto PCS [12]. The experiments showed that PCS is able to remove more than 80% of anionic dyes from aqueous solutions. The removal of Reactive Red 195 as versatile textile anionic dye has been investigated by using adsorption onto PCS [13]. The results indicate that PCS can be used as an effective and low-cost biosorbent for removal of reactive dyes from aqueous solution. The ability of PCS for the removal of cationic dye methylene blue from aqueous solutions was confirmed through batch adsorption experiments [14]. PCS has been also used for the removal of inorganic pollutants from aqueous solutions. The study of Pb^{2+} adsorption onto PCS showed that the adsorption efficiency is highly dependent on the solution pH so that it decreased from 53.6% at pH 4.0 to 6.73% at pH 2.0 [15]. At optimum pH, the loading capacity of PCS for Pb^{2+} increased from 1.23 to 8.30 mg/g by increasing the initial concentration from 10 to 100 mg/L. PCS has been also used for Cu^{2+} removal from aqueous solutions [16]. The results showed that it can be used as a novel and an effective adsorbent for the removal of Cu^{2+} from aqueous solutions. The removal of chromium(VI) from aqueous solution was investigated by PCS [17]. Cr(VI) is primarily present in industrial waste as chromate (CrO_4^{2-}) and dichromate ($\text{Cr}_2\text{O}_7^{2-}$) anionic species. The loading capacity of PCS for Cr(VI) increased from 50 to 201.8 mg/g by increasing the initial concentration from 50 to 300 mg/L. Furthermore, the biosorption was rapid with 84% of the total adsorption occurring in 2 h [17]. Although the adsorption efficiency of various pollutants onto PCS has been confirmed, but no work has been reported on the use of PCS for the removal of CN^- from aqueous solutions. Therefore, the present study is aimed to investigate a convenient and economic method for free cyanide removal from aqueous solutions by adsorption onto PCS as a low-cost and an abundantly available adsorbent.

2. Materials and methods

2.1. Reagents

The analytical reagent grade NaCN, AgNO_3 , KI and NaOH were obtained from Merck Co., Germany. Pine cones were collected from pine trees of the campus of university of Birjand. Their length was in the range of 5.5–8.5 cm. The scales were picked up from the pine cones by using a cutter, washed with double distilled water several times, dried at 70°C for 24 h and used in the adsorption experiments. The length of PCSs was in the range of 2.5–3.2 cm and their width was in the range of 1.5–2.3 cm.

2.2. Analysis methods

The CN concentration in the solution was determined by titration using standard silver nitrate solution in the presence of potassium iodide as indicator. The chemical composition of the PCS sample was determined by Elemental Combustion System 4010 CHNS-O Analyzer, Costech Analytical Technologies Inc., USA. Infrared spectra of the PCS sample before and after CN adsorption were recorded on a JASCO FT/IR-4600 spectrometer. Philips XL30 scanning electron microscope in the BSE imaging mode was used to obtain high-resolution compositional maps of the PCS sample. SEM images were taken in SE imaging mode to provide information on the morphology and surface topography of the PCS sample. WDX studies were carried out with a WDX 3PC, MICROSPEC Corp., USA. The porous properties of the sample were determined by Belsorp mini II surface area and pore size analyzer through determining its N_2 adsorption and desorption isotherms at 77 K. The sample was degassed at 110°C in a vacuum condition prior to gas adsorption measurements.

2.3. Adsorption experiments

In order to determine the loading capacity of the adsorbent, 10 g PCS was added into the 500 mL CN^- containing solution and agitated at constant rotation speed of 100 rpm by bottle roll apparatus for 76 h. The test was performed at ten different initial CN^- concentrations in the range of 26.54 to 530.89 mg/L. The solution pH was pre-adjusted at 10 by using 1 M NaOH solution and the solution temperature was kept constant at $20 \pm 1^\circ\text{C}$ during the experiments. After equilibrium, sampling was performed by removing 2 mL aliquots and they were analyzed for CN^- . The q_e and removal percentage were determined by Eq. (1) and Eq. (2), respectively.

$$q_e = \frac{(c_0 - c_e)V}{W} \quad (1)$$

$$\text{Removal\%} = \frac{c_0 - c_e}{c_0} \times 100 \quad (2)$$

Kinetic experiments were carried out similar to the equilibrium tests. Only sampling was done at predetermined time intervals during the adsorption process. The q_t values were calculated using Eq. (3).

$$q_t = \frac{(c_0 - c_t)V}{W} \quad (3)$$

3. Results and discussion

3.1. Characterization of PCS

Fig.1 shows the CHNS-O spectrum of the PCS sample. Three peaks at retention times around 1.25, 2.10 and 7.86 min are observed which are referred to nitrogen, carbon and hydrogen elements, respectively. The major peak is observed at retention time around 2.10 min which is related to carbon element. The chemical composition of the PCS by CHNS-O analysis was determined to be 48.91% carbon, 6.12% hydrogen, 0.5% nitrogen, 44.47% oxygen and with-

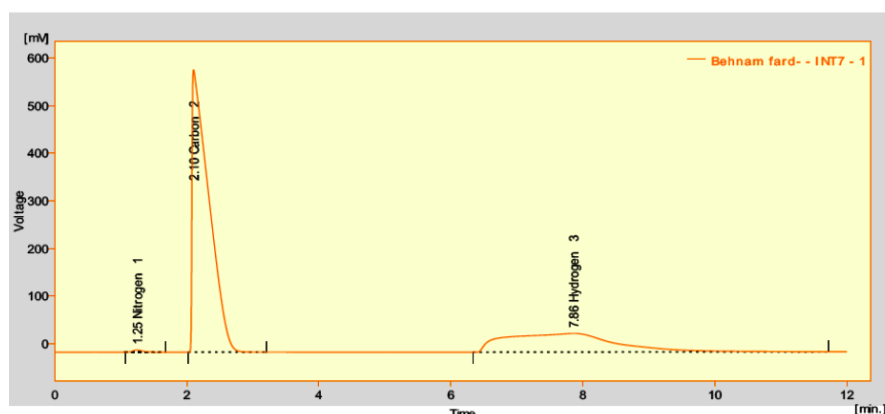


Fig. 1. CHNO-S spectrum of the PCS sample.

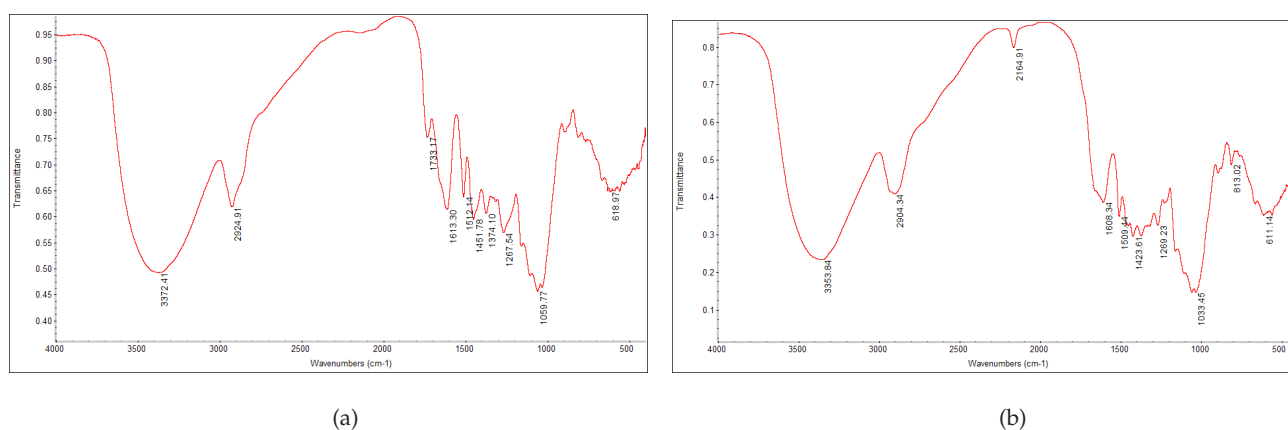


Fig. 2. FTIR spectrum of the PCS sample (a) before and (b) after adsorption of CN^- .

out sulfur. It can be revealed that the PCS is a carbon-based material containing a considerable amount of oxygen and hydrogen. The carbon atoms at the edge of the aromatic sheets have unsaturated valences and can therefore react with heteroatoms such as oxygen and produce different surface functional groups such as carboxylic, lactone, phenol, carbonyl, pyrone, chromene, quinone, and ether groups [18,19]. It was proposed that certain oxygen containing surface functionalities such as carboxylic acid or carboxylic anhydride, lactone, and phenolic hydroxyl can contribute to the carbon acidity. Furthermore, functional groups such as quinone, chromene, ketone, and pyrone have been postulated as the sources of surface basicity [18,19].

The FTIR analysis was used to detect different surface functional groups on the PCS surface. Fig. 2a shows the FTIR spectrum of the PCS sample. The carboxylic acid surface functional group can be distinguished from the peak at 1733.17 cm^{-1} as a result of C=O bond stretching vibration and the peak at 3372.41 cm^{-1} as a result of O-H stretching vibration. The phenolic groups can be detected from the peaks at 1059.77 , 1107.14 and 1267.54 cm^{-1} due to C-O stretching vibration and the peak at 3372.41 cm^{-1} as a result of O-H stretching vibration. The quinone group can be distinguished from the peak observed at 2924.91 cm^{-1} due to asymmetric and symmetric C-H stretching vibrations. The

peaks appeared at 1613.30 and 1733.17 cm^{-1} as a result of C=O bond stretching vibration can be responsible for the presence of ketone group on the PCS surface. Hence, both of acidic and basic surface functional groups are present on the PCS surface.

Fig. 3a shows the surface topography of the PCS sample. It can be seen that PCS contains many pores of different size inside. SEM image of the sample in BSE imaging mode has been shown in Fig. 3b. BSE imaging mode is used to detect contrast between areas with different chemical compositions. A “brighter” BSE intensity correlates with greater average atomic number in the sample, and “darker” areas have lower average atomic number. As can be seen in this figure, one phase can be detected based on BSE intensity and darker areas in this figure are related to pores. The map of distribution and relative proportion of carbon element over the scanned area is shown in Fig. 3c. It is clear that by ignoring the pore areas, the carbon element is distributed over the all scanned area. This further confirms that the PCS is a carbon-based material.

The porous properties of the sample were investigated by using high precision surface area and pore size analyzer. The results showed that the BET surface area, total pore volume and average pore diameter of the sample are $0.657\text{ m}^2/\text{g}$, $0.020114\text{ cm}^3\text{ g}^{-1}$ and 122.41 nm , respectively. Fig. 4

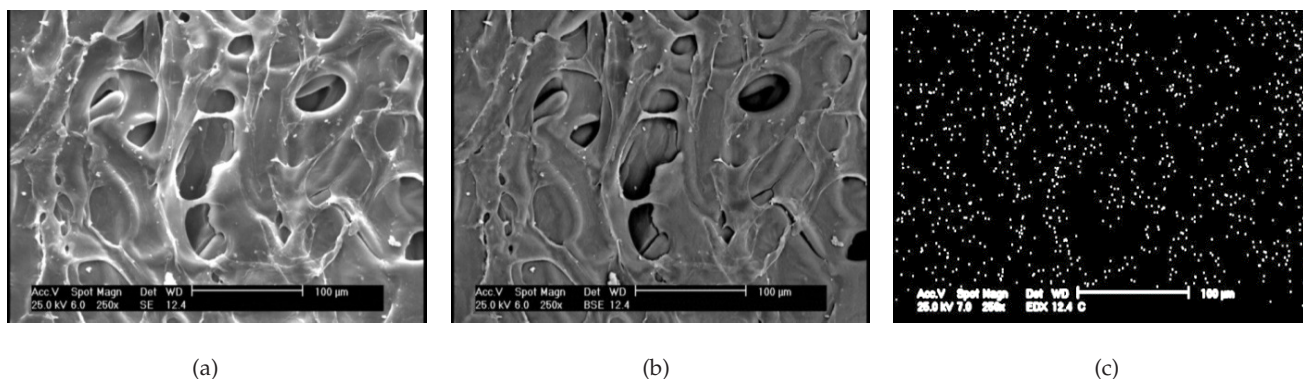


Fig. 3. SEM photographs of PCS in (a) SE imaging mode and (b) BSE imaging mode (c) Map of distribution and relative proportion of carbon element over the scanned area.

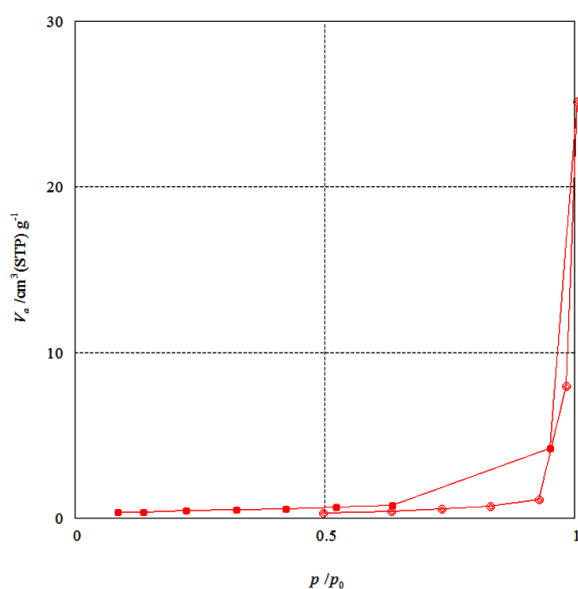


Fig. 4. Adsorption/desorption isotherms for N_2 gas onto PCS at 77K.

shows the N_2 adsorption and desorption isotherm onto the PCS at 77K. This isotherm is convex to the relative pressure, p/p_0 axis over its entire range. It resembles to the Type III of the five main types of adsorption isotherms which proposed by IUPAC. This type of adsorption isotherm indicates unrestricted multilayer formation process [20]. It forms since lateral interactions between adsorbed molecules are strong in comparison to interactions between the adsorbent surface and adsorbate. Type III isotherm is the normal form of isotherm obtained with a macroporous adsorbent [20].

3.2. Adsorption capacity of PCS for CN^-

In order to investigate the initial CN^- concentration on the loading capacity and removal percentage, 10 g PCS was added into 500 mL solution pre-adjusted pH at 10 and containing exact amount of CN^- in the range of 26.54–530.89 mg/L. Afterward, it was kept rotating at a speed of 100 rpm by bottle roll apparatus for 76 h to establish the equilibrium. The results are presented in Fig. 5. As can be seen, the removal percentage decreased from 87.5% to 25% by

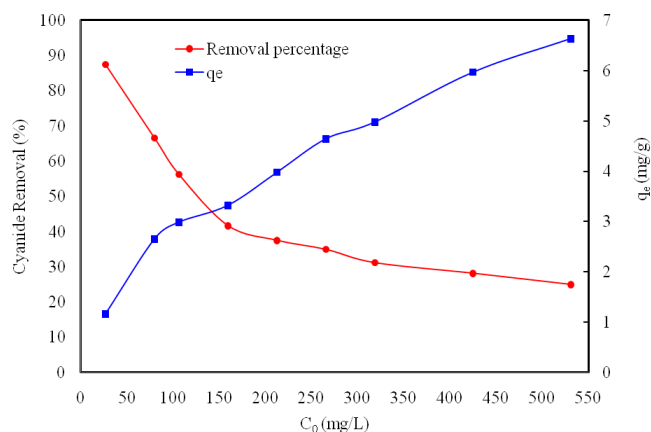


Fig. 5. Effect of initial CN^- concentration on the CN^- removal percentage and adsorption capacity of PCS (conditions: sorbent dosage = 10 g (500 mL) $^{-1}$; stirring speed = 100 rpm; $T = 20 \pm 1^\circ C$; pH 10; Time = 76 h).

increasing initial CN^- concentration from 26.54 to 530.89 mg/L. This may be due to the saturation of the adsorption sites at higher CN^- concentrations. Meanwhile, the amount of CN^- adsorption at equilibrium (q_e) increased from 1.16 to 6.64 mg/g by increasing initial CN^- concentration from 26.54 to 530.89 mg/L. The initial CN^- concentration provides an important driving force to overcome all mass transfer resistance. Hence, a higher initial concentration of CN^- tends to enhance the adsorption capacity. A similar phenomenon was observed for the adsorption of CN^- onto the activated carbon [4–6].

A review on the loading capacity of various biosorbents for CN^- was made and the results are presented in Table 1. As can be seen the loading capacity of activated carbon in the plain form is in the range of 2.5–20 mg/g and its impregnation with metal cations such as copper and silver increases the loading capacity more than twice. Nonetheless, some of argo-based material such as almond shell and sagwan leaves have higher loading capacity in comparison with plain activated carbon. The loading capacity of PCS for CN^- is in the range of plain activated carbon and it is greater than some kinds of biomass such as rice husk.

In order to confirm the loading of CN^- onto PCS and discover the adsorption mechanism, the FTIR analysis were performed on the PCS sample before and after adsorption

Table 1
A review on the loading capacity of various biosorbents for CN⁻

Adsorbent		q_e (mg/g)	Ref.
Activated carbon	Plain	7.8	[4]
	Ni-impregnated	15.4	
	Ag-impregnated	26.3	
Activated carbon	Plain	19.7	[5]
	Cu-impregnated	22.4	
	Ag-impregnated	29.6	
Activated carbon	Plain	2.568	[6]
	Cu-impregnated	6.389	
	Ag-impregnated	18.094	
Sagwan leaves		18.45	[7]
Rice husk		1.957	[6]
Almond Shell		32.05	[7]
Calcinated eggshells		3.27	[8]
Coke	Raw	1.2	[9]
	KMnO ₄ Oxidized	1.28	
Pine cone Scale (PCS)		6.64	Current study

of CN⁻ and the results are presented in Fig. 2. The distinct difference between the two spectra is the prominent peak at 2164.91 cm⁻¹ (after CN⁻ adsorption) which can be assigned to CN triple bond stretching vibrations. It confirms the adsorption of CN⁻ by PCS. As previously mentioned, the peak observed at 2924.91 cm⁻¹ due to asymmetric and symmetric C–H stretching vibrations is indicative of quinone group on the PCS surface. Furthermore, the peaks appeared at 1613.30 and 1733.17 cm⁻¹ as a result of C=O bond stretching vibrations are indicative of ketone group on the PCS surface. Quinone groups may be responsible for the adsorption of CN⁻ onto PCS since wave number shifted from 2924.91 cm⁻¹ (before CN⁻ adsorption) to 2904.34 cm⁻¹ (after CN⁻ adsorption). Ketone groups are also responsible for CN⁻ adsorption onto PCS since wave number shifted from 1613.30 cm⁻¹ (before CN⁻ adsorption) to 1608.34 cm⁻¹ (after CN⁻ adsorption) and the peak at 1733.17 cm⁻¹ has weakened after CN⁻ adsorption. These suggest that the adsorption of CN⁻ onto PCS occurs by basic surface functional groups via ion exchange mechanism. The other researchers assumed the same mechanism for CN⁻ adsorption onto the carbon-based adsorbents [7,21,22].

3.3. Modeling of the equilibrium data

Modeling of the equilibrium data is a necessary way for predicting the performance of adsorption processes, which is essential for designing and optimizing purposes [23]. The equilibrium data were fitted with different two-parameter isotherm models including FIM, LIM, TIM [21]. Eq. (4) shows the FIM.

$$q_e = K_F(C_e)^{1/n} \quad (4)$$

The well-known form of LIM is represented in Eq. (5).

$$q_e = (q_{mL}K_L C_e)/(1+K_L C_e) \quad (5)$$

Eq. (6) shows the TIM.

$$q_e = q_{mT} \ln(K_T C_e) \quad (6)$$

The equilibrium data were also modeled by three-parameter isotherm models including RPIM and KCIM. The well-known form of RPIM and KCIM are presented in Eq. (7) and Eq. (8), respectively.

$$q_e = (A_{RP} C_e)/(1 + B_{RP} C_e^S) \quad (7)$$

$$q_e = (A_{KC} C_e^P)/(1 + B_{KC} C_e^P) \quad (8)$$

The modeling of equilibrium data was carried out by LRM. In this method, the isotherm parameters can be determined from linear forms of the isotherm models. In the case of RPIM and KCIM isotherms, the constants A_{RP} and P were obtained by minimizing the ARE value using a trial and error method. The ARE value can be defined as:

$$ARE = \frac{100}{N} \sum_{i=1}^N \left| \frac{(q_e^{\text{exp}} - q_e^{\text{cal}})}{q_e^{\text{exp}}} \right|_i \quad (9)$$

The smaller ARE value indicates more accurate estimation of q_e value.

In this research, the equilibrium data was modeled apart from LRM by NLRM. In order to determine the isotherm parameters by NLRM, a trial and error procedure was developed which is applicable by using a computer operation. Therefore, an optimization procedure is adopted in solving the equations by approaching the ARE value to zero by using the solver add-in function of the Microsoft excel.

Table 2 summarizes the corresponding isotherm parameters and the related R² and ARE values by using LRM. As can be seen, the FIM fitted the equilibrium data better than the other two-parameter isotherm models. The FIM proposes that the PCS surface is heterogeneous and the stronger binding sites are occupied first and the binding strength decreases by increasing adsorption site occupation. Furthermore, it suggests that there is interaction between the adsorbed ions. The FIM constant, n , is related to the adsorption intensity, so that the lower fractional value of $1/n$ [$0 < (1/n) < 1$] indicates weak adsorptive forces are effective on the surface of adsorbent [24]. The value of $1/n$ was determined 0.3501 which is in the range of 0.1 to 1. It reveals that the adsorption process is favorable and the surface heterogeneity is considerable. As can be seen, the RPIM has the lowest ARE value among the other isotherm models. It indicates that the equilibrium data for the adsorption of CN⁻ onto the PCS is best represented by the RPIM.

Fig. 6 shows plot of the experimental q_e values against the predicted q_e values by various isotherm models by using NLRM. As can be shown, the FIM, RPIM and KCIM can generate a satisfactory fit to the experimental data. The parameters of the isotherm models by NLRM as well as the related ARE values are given also in Table 2. It can be seen that the FIM, RPIM and KCIM have nearly the same ARE value. It indicates that these isotherm models can model the equilibrium data better than the other isotherm models. However, the RPIM exhibited the lowest ARE value, which

Table 2
Parameters of isotherm models by LRM and NLRM for the adsorption of CN⁻ onto PCS

Isotherms	LRM			NLRM	
	R ²	ARE	Parameters	ARE	Parameters
FIM	0.9845	5.359	$K_F = 0.768 \text{ (mg g}^{-1}) \text{ (L mg}^{-1})^{1/n}$; $n = 2.856$	4.770	$K_F = 0.762 \text{ (mg g}^{-1}) \text{ (L mg}^{-1})^{1/n}$; $n = 2.845$
LIM	Type(I)	0.9406	19.144	17.312	$q_{mL} = 4.246 \text{ (mg g}^{-1})$; $K_L = 0.113 \text{ (L mg}^{-1})$
	Type(II)	0.9359	17.838		
	Type(III)	0.5829	18.635		
	Type(IV)	0.5829	20.158		
TIM	0.8843	15.380	$q_{mT} = 1.08 \text{ (mg g}^{-1})$; $K_T = 0.494 \text{ (L mg}^{-1})$	10.463	$q_{mT} = 0.765 \text{ (mg g}^{-1})$; $K_T = 1.377 \text{ (L mg}^{-1})$
RPIM	0.9954	4.762	$g = 0.657$; $B_{RP} = 11.408 \text{ (L mg}^{-1})^g$; $A_{RP} = 9.127 \text{ (mg g}^{-1}) \text{ (L mg}^{-1})$	4.729	$g = 0.658$; $B_{RP} = 11.396 \text{ (L mg}^{-1})^g$; $A_{RP} = 9.134 \text{ (mg g}^{-1}) \text{ (L mg}^{-1})$
KCIM	0.9859	5.316	$A_{KC} = 0.746 \text{ (mg g}^{-1}) \text{ (L mg}^{-1})^P$; $B_{KC} = -0.116 \text{ (L mg}^{-1})^P$; $P = 0.2501$	4.752	$A_{KC} = 0.762 \text{ (mg g}^{-1}) \text{ (L mg}^{-1})^P$; $B_{KC} = 2.26E-5 \text{ (L mg}^{-1})^P$; $P = 0.351$

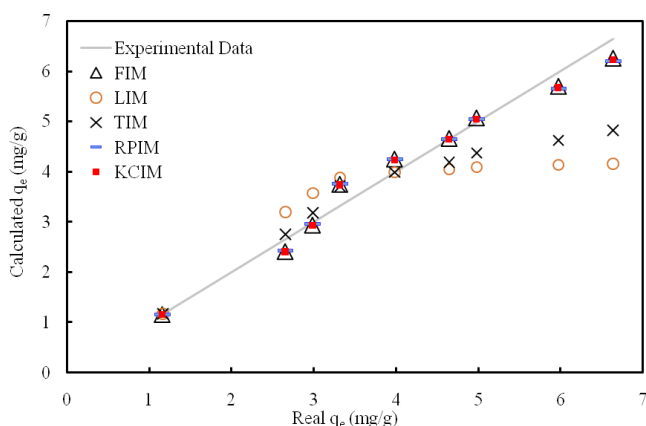


Fig. 6. The predicted q_e values by NLRM versus experimental q_e values for the adsorption of CN⁻ onto PCS.

produced a considerably better fit compared with the other isotherms.

3.4. Adsorption kinetics of CN⁻ onto PCS

The adsorption kinetics is one of the criteria for the efficiency evaluation of an adsorbent. Furthermore, the adsorption mechanism can be concluded from kinetic studies. The adsorption kinetics of CN⁻ onto PCS was investigated at three different initial CN⁻ concentrations and the results are presented in Fig. 7. It can be seen that the rate of adsorption is higher at beginning and reduces gradually. This is probably due to higher adsorption sites being available at beginning for the adsorption of CN⁻. The amount of CN⁻ adsorption increases with time and it remains constant after equilibrium at different initial CN⁻ concentrations.

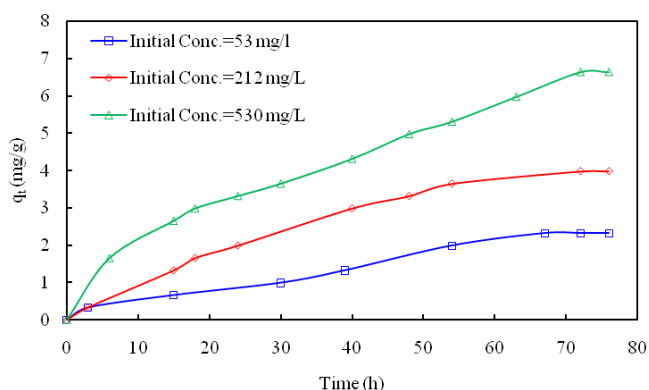


Fig. 7. The adsorption kinetics of CN⁻ onto PCS at three different initial CN⁻ concentrations of 53, 212 and 530 mg/L (conditions: sorbent dosage = 10 g (500 mL)⁻¹; stirring speed = 100 rpm; T = 20±1°C; pH 10).

3.5. Modeling of the kinetic data

Modeling of the kinetic data was carried out using EKM, FPKM, PFOKM and PSOKM [21,25]. The general form of EKM is represented in Eq. (10).

$$q_t = \beta^{-1} \ln(\alpha\beta) + \beta^{-1} \ln t \quad (10)$$

Eq. (11) shows the FPKM.

$$q_t = kt^v \quad (11)$$

The PFOKM is generally expressed as Eq. (12).

$$q_t = q_{PFO} [1 - \exp(-k_1 t)] \quad (12)$$

Eq. (13) shows the PSOKM.

$$q_t = \frac{t}{(1/k_2q_{PSO}^2) + (t/q_{PSO})} \tag{13}$$

The modeling of the kinetic data was done by LRM and NLRM. The ability of kinetic models to describe the adsorption process, apart from the R^2 , was further validated by the *ARE* value. In LRM, the constant parameters of the kinetic models can be determined through the slope and intercept of linear plot of kinetic equations. The PSOKM can be linearized into four different types and the model constants can be obtained from each of the following plots: $[t/q_t \text{ vs. } t]$, $[1/q_t \text{ vs. } 1/t]$, $[q_t \text{ vs. } q_t/t]$, $[q_t/t \text{ vs. } q_t]$. Furthermore, by plotting q_t against $\ln t$, the EKM constant of β and α can be determined, by plotting $\ln q_t$ against $\ln t$, the FPKM constant of k and v can be obtained and by plotting $\ln(q_e - q_t)$ against t , the PFOKM constant of q_{ePFO} and k_{1p} can be calculated from the slope and intercept.

The values of R^2 , *ARE* and parameters of different kinetic models for adsorption of CN^- onto PCS at 212 mg/L initial CN^- concentration by using LRM are listed in Table 3. It was found that the fitting to PSOKM gave the highest value of R^2 , the lowest value of *ARE* and the predicted q_e more accurately than the other three models investigated. Therefore, the PSOKM could be used for the prediction of the kinetics of CN^- adsorption onto PCS. Among the linear expressions of PSOKM, Type III was found to be the most appropriate rate expression.

For NLRM, a trial and error procedure, which is applicable to computer operation, was developed and used to determine the kinetic parameters by minimizing the respective *ARE* value using the solver add-in function of the Microsoft excel. Fig. 8 shows the ability of different kinetic models to predict the adsorption kinetics of CN^- onto PCS by using NLRM. It can be seen that PSOKM fits the experimental data better than the other kinetic models. Table 3 also shows the *ARE* values and the parameters of different kinetic models for the adsorption of CN^- onto

PCS by NLRM. The results indicate that the PSOKM gives the most accurate predictions of the adsorption kinetics of CN^- onto PCS.

3.6. Adsorption mechanism

It is well-known that the overall adsorption rate in a porous adsorbent must consider the three following steps: external mass transport or film diffusion, intraparticle diffusion and adsorption on an active site inside the pores. The overall rate of adsorption is controlled by either film or intraparticle diffusion, or a combination of both mechanisms [26]. The WMIDM, in which the rate of intraparticle diffusion is a function of $t^{0.5}$ can be defined as follows [27]:

$$q_t = k_p t^{0.5} + x \tag{14}$$

Weber and Morris proposed that if intraparticle diffusion was involved in the adsorption process, then a plot of

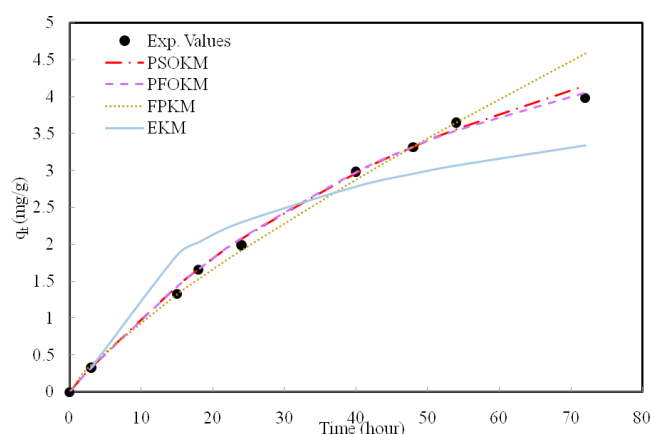


Fig. 8. The predicted q_t values vs. experimental q_t values for the adsorption of CN^- onto PCS by NLRM.

Table 3
Parameters of kinetic models by LRM and NLRM for the adsorption of CN^- onto PCS at 212 mg/L initial CN^- concentration

Kinetic models	LRM			NLRM	
	R^2	<i>ARE</i>	Parameters	<i>ARE</i>	Parameters
EKM	0.9202	29.755	$\beta = 0.830 \text{ (g mg}^{-1}\text{)}$; $\alpha = 0.357 \text{ (mg g}^{-1} \text{h}^{-1}\text{)}$	15.913	$\beta = 1.055 \text{ (g mg}^{-1}\text{)}$; $\alpha = 0.448 \text{ (mg g}^{-1} \text{h}^{-1}\text{)}$
FPKM	0.9916	5.488	$k = 0.149 \text{ (mg g}^{-1} \text{h}^{-v}\text{)}$; $v = 0.801$	5.269	$k = 0.154 \text{ (mg g}^{-1} \text{h}^{-v}\text{)}$; $v = 0.793$
PFOKM	0.9576	38.610	$q_{PFO} = 4.646 \text{ (mg g}^{-1}\text{)}$; $k_{1p} = 0.043 \text{ h}^{-1}$	2.459	$q_{PFO} = 5.120 \text{ (mg g}^{-1}\text{)}$; $k_{1p} = 0.022 \text{ h}^{-1}$
PSOKM	Type(I)	0.9766	$q_{PSO} = 8.326 \text{ (mg g}^{-1}\text{)}$; $k_{2p} = 0.002 \text{ (g mg}^{-1} \text{h}^{-1}\text{)}$	2.435	$q_{PSO} = 8.295 \text{ (mg g}^{-1}\text{)}$; $k_{2p} = 0.001674 \text{ (g mg}^{-1} \text{h}^{-1}\text{)}$
	Type(II)	0.9995	$q_{PSO} = 7.651 \text{ (mg g}^{-1}\text{)}$; $k_{2p} = 0.002 \text{ (g mg}^{-1} \text{h}^{-1}\text{)}$		
	Type(III)	0.9551	$q_{PSO} = 8.206 \text{ (mg g}^{-1}\text{)}$; $k_{2p} = 0.002 \text{ (g mg}^{-1} \text{h}^{-1}\text{)}$		
	Type(IV)	0.9551	$q_{PSO} = 8.470 \text{ (mg g}^{-1}\text{)}$; $k_{2p} = 0.002 \text{ (g mg}^{-1} \text{h}^{-1}\text{)}$		

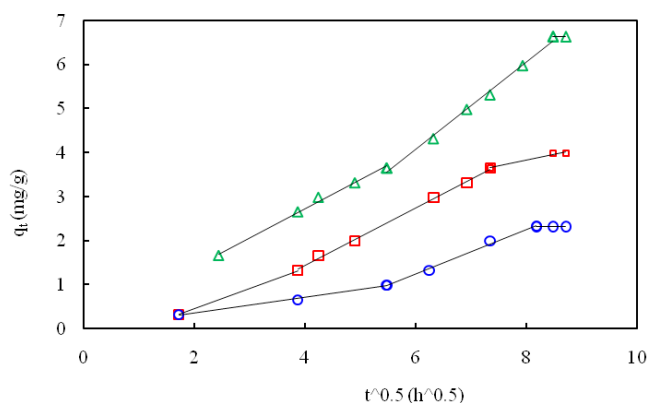


Fig. 9. Weber–Morris plots for CN^- adsorption onto PCS at different initial CN^- concentrations of 53 mg/L (O), 212 mg/L (□) and 530 mg/L (△) (conditions: sorbent dosage = 10 g (500 mL) $^{-1}$; stirring speed = 100 rpm; T = 20±1°C; pH 10).

$t^{0.5}$ vs. q_t would result in a linear relationship, and that the intraparticle diffusion would be the controlling step if this line passes through the origin [27].

Fig. 9 shows the Weber and Morris plots for the adsorption of CN^- onto PCS at three different initial CN^- concentrations. It is clear that the plots of q_t versus $t^{0.5}$ are not a straight line through the full range of contact time. However, a much more precise observation revealed that the data points can be divided into two or three linear sections with different slopes (i.e. k_p value). This suggests that the overall rate of adsorption is controlled by a combination of both film and intraparticle diffusion mechanisms. Fig. 9 also shows that the linear plot did not pass through the origin which indicates that the intraparticle diffusion is not the sole rate controlling step and the film diffusion controlled the adsorption at beginning.

4. Conclusion

The characterization of the PCS sample showed that it is a carbon-based adsorbent and different acidic and basic surface functional groups there are on its surface. The surface area and mean pore diameter of the sample was determined to be 0.657 m²/g and 122.41 nm, respectively. The adsorption of CN^- was found to be dependent on the initial CN^- concentration so that it increases from 1.16 to 6.64 mg/g by increasing the initial CN^- concentration from 26.5 to 530.9 mg/L. The removal percentage of CN^- decreases from 87.5% to 25% by increasing initial CN^- concentration from 26 to 530 mg/L. The basic surface functional groups present on the PCS surface adsorb CN^- ions through ion exchange mechanism. The equilibrium adsorption data were represented by FIM better than LIM which indicates that the PCS surface is heterogeneous, there is interaction between adsorbed ions and the adsorption energy exponentially decreases upon completion of the sorption sites. The equilibrium data for the adsorption of CN^- onto the PCS were best represented by RPIM. The adsorption kinetics was described well by PSOKM. The intraparticle diffusion was not the sole rate controlling step of the adsorption process and the process is film diffusion control to much extent.

Acknowledgement

The authors of the paper express their deep gratitude to the research and technology affairs of University of Birjand for providing some of the project costs. The authors declare that they have no conflict of interest.

Symbols

A_{RP}	— RPIM constant, ((mg g ⁻¹) (L mg ⁻¹))
AVR	— Acidification Volatilization Recovery
B_{RP}	— RPIM constant, ((L mg ⁻¹) ^g)
C_0	— Initial cyanide ion concentration, (mg/L)
C_t	— Cyanide ion concentration at time t, (mg/L)
C_e	— Equilibrium cyanide ion concentration, (mg/L)
CN	— Cyanide
CN^-	— Cyanide Ion
EKM	— Elovich Kinetic Model
FIM	— Freundlich Isotherm Model
FPKM	— Fractional Power Kinetic Model
FTIR	— Fourier-transform infrared
g	— RPIM constant
IUPAC	— International Union of Pure and Applied Chemistry
k	— FPKM constant, (mg g ⁻¹ h ^{-v})
k_{1p}	— PFOKM constant, (h ⁻¹)
k_{2p}	— PSOKM constant, (g mg ⁻¹ h ⁻¹)
KCIM	— Koble-Corrigan Isotherm Model
K_F	— FIM constant, ((mg g ⁻¹) (L mg ⁻¹) ^{1/n})
K_L	— LIM constant, (L mg ⁻¹)
k_p	— Rate constant for the intraparticle diffusion, (mg g ⁻¹ h ^{-1/2})
K_T	— TIM constant, (L mg ⁻¹)
LIM	— Langmuir Isotherm Model
LRM	— Linear Regression Method
n	— FIM constant
N	— Number of measurements made
NLRM	— Non-Linear Regression Method
PCS	— Pine Cone Scale
PFOKM	— Pseudo First Order Kinetic Model
PSOKM	— Pseudo Second Order Kinetic Model
q_e	— The amount of adsorption at equilibrium, (mg/g)
q_e^{cal}	— Calculated amount of CN^- adsorbed on the PCS, (mg/g)
q_e^{exp}	— Experimental amount of CN^- adsorbed on the PCS, (mg/g)
q_{mL}	— LIM constant, (mg g ⁻¹)
q_{mT}	— TIM constant, (mg g ⁻¹)
q_{PFO}	— PFOKM constant, (mg g ⁻¹)
q_{PSO}	— PSOKM constant, (mg g ⁻¹)
q_t	— The amount of adsorption at time t, (mg/g)
R^2	— Correlation coefficient
RPIM	— Redlich–Peterson Isotherm Model
SE	— Secondary Electron
SEM	— Scanning Electron Microscopy
T	— Time, (h)
TIM	— Temkin Isotherm Model
v	— FPKM constant
V	— Volume of solution, (L)
W	— Mass of the adsorbent, (g)

WDX	— Wave Length Dispersive X-ray
WMIDM	— Weber and Morris's Intraparticle Diffusion Model
x	— WMIDM constant, (mg/g)
α	— EKM constant, (mg g ⁻¹ h ⁻¹)
β	— EKM constant, (g mg ⁻¹)

References

- [1] R.R. Dash, A. Gaur, C. Balomajumder, Cyanide in industrial wastewaters and its removal: A review on biotreatment, *J. Hazard. Mater.*, 163 (2009) 1–11.
- [2] N. Gupta, C. Balomajumder, V.K. Agarwal, Adsorption of cyanide ion on pressmud surface: A modeling approach, *Chem. Eng. J.*, 191 (2012) 548–556.
- [3] E. Jaszczak, Z. Polkowska, S. Narkowicz, J. Namieśnik, Cyanides in the environment—analysis—problems and challenges, *Environ. Sci. Pollut. Res.*, 24 (2017) 15929–15948.
- [4] N. Adhoum, L. Monser, Removal of cyanide from aqueous solution using impregnated activated carbon, *Chem. Eng. Process.*, 41 (2002) 17–21.
- [5] H. Deveci, E.Y. Yazıcı, I. Alp, T. Uslu, Removal of cyanide from aqueous solutions by plain and metal-impregnated granular activated carbons, *Int. J. Miner. Process.*, 79 (2006) 198–208.
- [6] E.Y. Yazıcı, H. Deveci, I. Alp, Treatment of cyanide effluents by oxidation and adsorption in batch and column studies, *J. Hazard. Mater.*, 166 (2009) 1362–1366.
- [7] N. Dwivedi, C. Balomajumder, P. Mondal, Comparative investigation on the removal of cyanide from aqueous solution using two different bioadsorbents, *Water Res. Ind.*, 15 (2016) 28–40.
- [8] O.A.A. Eletta, O.A. Ajayi, O.O. Ogunleye, I.C. Akpan, Adsorption of cyanide from aqueous solution using calcinated eggshells: Equilibrium and optimisation studies, *J. Environ. Chem. Eng.*, 4 (2016) 1367–1375.
- [9] Z. Hattab, N. Filali, R. Mazouz, K. Guerfi, N. Rebbani, A. Nafa, S. Kheriaf, Adsorption of cyanide ions in aqueous solution using raw and oxidized coke, *Desal. Water Treat.*, 57(8) (2016) 3522–3531.
- [10] A. Farjon, *A natural history of conifers*, Timber Press, Portland, Oregon, 2008.
- [11] A. Farjon, *A Handbook of the World's Conifers*, Brill press, Boston, 2010.
- [12] N.M. Mahmoodi, B. Hayati, M. Arami, C. Lan, Adsorption of textile dyes on Pine Cone from colored wastewater: Kinetic, equilibrium and thermodynamic studies, *Desalination*, 268 (2011) 117–125.
- [13] O. Aksakala, H. Ucun, Equilibrium, kinetic and thermodynamic studies of the biosorption of textile dye(Reactive Red 195) onto *Pinus sylvestris* L., *J. Hazard. Mater.*, 181 (2010) 666–672.
- [14] T.K. Sen, S. Afroze, H.M. Ang, Equilibrium, kinetics and mechanism of removal of methylene blue from aqueous solution by adsorption onto pine cone biomass of *Pinus radiata*, *Water Air Soil Pollut.*, 218 (2011) 499–515.
- [15] M. Momčilović, M. Purenović, A. Bojić, A. Zarubica, M. Randelović, Removal of lead(II) ions from aqueous solutions by adsorption onto pine cone activated carbon, *Desalination*, 276 (2011) 53–59.
- [16] A.O. Adeyemo, K.O. Adebawale, B.I. Olu-Owolabi, Adsorption of copper by raw pinecone, *Am. Chem. Sc. J.*, 4(6) (2014) 992–1000.
- [17] H. Ucun, Y.K. Bayhan, Y. Kaya, A. Cakici, O.F. Algur, Biosorption of chromium(VI) from aqueous solution by cone biomass of *Pinus sylvestris*, *Bioresource Technol.*, 85 (2002) 155–158.
- [18] R.C. Bansal, M. Goyal, *Activated Carbon Adsorption*, Taylor & Francis Group, USA, 2005.
- [19] M.S. Shafeeyan, W.M.A.W. Daud, A. Houshmand, A. Shamiri, A review on surface modification of activated carbon for carbon dioxide adsorption, *J. Anal. Appl. Pyrol.*, 89 (2010) 143–151.
- [20] M. Thommes, Physical adsorption characterization of nanoporous materials, *Chem. Ing. Tech.*, 82(7) (2010) 1059–1073.
- [21] A. Behnamfard, M.M. Salarirad, Equilibrium and kinetic studies on free cyanide adsorption from aqueous solution by activated carbon, *J. Hazard. Mater.*, 170 (2009) 127–133.
- [22] M. Fouladvand, B. Ramavandi, Adsorption potential of NH₄Br-soaked activated carbon for cyanide removal from wastewater, *Indian J. Chem. Technol.*, 22(5) (2015) 183–193.
- [23] K.Y. Foo, B.H. Hameed, Insights into the modeling of adsorption isotherm systems, *Chem. Eng. J.*, 156 (2010) 2–10.
- [24] H.A. Omar, H. Moloukhia, Use of activated carbon in removal of some radioisotopes from their waste solutions, *J. Hazard. Mater.*, 157 (2008) 242–246.
- [25] Y.S. Ho, G. McKay, Sorption of dye from aqueous solution by peat, *Chem. Eng. J.*, 70 (1998) 115–124.
- [26] O. Hamdaoui, E. Naffrechoux, Adsorption kinetics of 4-chlorophenol onto granular activated carbon in the presence of high frequency ultrasound, *Ultrason. Sonochem.*, 16 (2009) 15–22.
- [27] W.J. Weber, J.C. Morris, Kinetics of adsorption on carbon from solution, *J. Sanitary Eng. Div., Am. Soc. Civil Eng.*, 89 (1963) 31–60.